Title: Comparative study of extracellular recording methods for analysis of afferent sensory information: empirical modeling, data analysis and interpretation

Authors: F.D. Farfán, C. Soto-Sanchez, A.G. Pizá, A.L. Albarracín, J.H. Soletta, F.A. Lucianna, E. Fernandez

PII: S0165-0270(19)30076-7
DOI: https://doi.org/10.1016/j.jneumeth.2019.03.004
Reference: NSM 8260

To appear in: *Journal of Neuroscience Methods*

Received date: 13 November 2018
Revised date: 2 March 2019
Accepted date: 4 March 2019

Please cite this article as: Farfán FD, Soto-Sanchez C, Pizá AG, Albarracín AL, Soletta JH, Lucianna FA, Fernandez E, Comparative study of extracellular recording methods for analysis of afferent sensory information: empirical modeling, data analysis and interpretation, *Journal of Neuroscience Methods* (2019), https://doi.org/10.1016/j.jneumeth.2019.03.004

Cover Letter

The manuscript have been revised and edited for a better understanding of the text.

Research article

Comparative study of extracellular recording methods for analysis of afferent sensory information: empirical modeling, data analysis and interpretation

Farfán FD[a,b], Soto-Sanchez C[c,d], Pizá AG[a,b], Albarracín AL[a,b], Soletta JH[a,b], Lucianna FA[a,b] and Fernandez E[c,d]

[a]Laboratorio de Medios e Interfases (LAMEIN), Departamento de Bioingeniería, Facultad de Ciencias Exactas y Tecnología, Universidad Nacional de Tucumán, Tucumán, Argentina.

[b]Instituto Superior de Investigaciones Biológicas (INSIBIO), Consejo Nacional de Investigaciones Científicas y Técnicas (CONICET), Tucumán, Argentina.

[c]Bioengineering Institute, Miguel Hernández University (UMH), Alicante, Spain.

[d]Biomedical Research Networking center in Bioengineering, Biomaterials and Nanomedicine (CIBER-BBN), Zaragoza, Spain

Email addresses:

FFD: ffarfan@herrera.unt.edu.ar (Corresponding Author)

SSC: csoto@goumh.umh.es

PAG: piza.ag@gmail.com

AAL: anaalbarracin@gmail.com

SJH: jorge.soletta@gmail.com

LFA: facundolucianna@gmail.com

EFJ: efernandez@umh.es

Highlights

- A comparative study of two electrophysiological methods was made.
- The morphology of the evoked CAPs was analyzed by using an empirical model, which allowed:
  - Establishing anatomical/functional relations,
  - Highlights the most relevant features of nerve conduction in myelinated fibers,
  - Improve the interpretations of the results obtained from each methodological approach,
  - Establish alternative hypotheses and,
  - Make inferences about the global functional aspects of the system,
- Functional characterizations were made according to the stimuli directions by using different processing techniques.

Abstract

Background. Physiological studies of sensorial systems often require the acquisition and processing of data extracted from their multiple components to evaluate how the neural information changes in relation to the environment changes. In this work, a comparative study about methodological aspects of two electrophysiological approaches is described.

New Method. Extracellular recordings from deep vibrissal nerves were obtained by using a customized microelectrode Utah array during passive mechanical stimulation of rat´s whiskers. These recordings were compared with those obtained with bipolar electrodes. We also propose here a simplified empirical model of the electrophysiological activity obtained from a bundle of myelinated nerve fibers.

Results. The peripheral activity of the vibrissal system was characterized through the temporal and spectral features obtained with both recording methods. The empirical model not only allows the correlation between anatomical structures and functional features, but also allows to predict changes in the CAPs morphology when the arrangement and the geometry of the electrodes changes.

Comparison with Existing Method(s). This study compares two extracellular recording methods based on analysis techniques, empirical modeling and data processing of vibrissal sensory information.

Conclusions. This comparative study reveals a close relationship between the electrophysiological techniques and the processing methods necessary to extract sensory information. This relationship is the result of maximizing the extraction of information from recordings of sensory activity.

Keywords

Extracellular recording, empirical modeling, bipolar electrodes, microelectrode array, data processing

Introduction

Nowadays, some studies in neuroscience involve different methodologies aimed at obtaining the greatest amount of information from the biological system and inferring about functional and global aspects of the system (Vertes and Stackman, 2011). However, in neurophysiology the interpretation of the results may not be easy in some cases and could lead to wrong conclusions.

The study of peripheral nerves activity and the interpretation of recordings obtained from them require considerations about conduction velocity, sensory threshold, neuronal coding/decoding and the nerve fibers types and distribution, among others (Ruch, 1973). Emerging methodologies have been used efficiently for the same purpose, such as cellular and molecular methods, invasive and non-invasive imaging, optogenetic and others (Merighi and Carmignoto, 2002; Rangavajla et al, 2014; Mohanty and Lakshminarayananan, 2015). However, few times have the electrophysiological methods been overcome by more sophisticated methodologies due to their simplicity and versatility (Vogt, 2018). In the last few years, these methods have evolved and achieved a greater versatility and applicability in different areas of neuroscience. This has been possible due to technological improvements in spatial (miniaturization and integration) and temporal resolution of the electrodes.

In this study, the methodological procedures of two electrophysiological techniques are compared and implemented to characterize functional aspects of the vibrissal system (Brecht et al, 1997; Krupa et al, 2001; Kleinfeld et al, 2006). They are

the classical bipolar extracellular recording (Albarracín et al, 2006) and the multichannel extracellular recording with a microelectrode array (MEA) (Branner and Normann, 2000).

The classical approach used to characterize the vibrissal system of rodents consisted in evoking activity by passive stimulation at the different nuclei throughout the sensorial pathway. Several studies have addressed these issue extracting information from the different stages of the pathwaw: at the trigeminal ganglion (Zucker and Welker, 1969; Gibson and Welker, 1983; Lichtenstein et al, 1990; Shoykhet et al, 2000), the trigeminal nuclei (Gibson, 1987; Nicolelis et al, 1995), the thalamus (Simons and Carvell, 1989; Castro-Alamancos, 2002), and the somatosensory cortex (Kyriazi et al, 1994; Nicolelis et al, 1995; Ahissar et al, 2000). In general, these approaches contributed to posterior studies about neural coding in active touch. However, the study of this sensorial system at peripheral level represents a serious methodological challenge since a variety of responses are evoked when the whiskers are passively stimulated (Mitchinson et al, 2004; Kwegyir-Afful et al, 2008; Lotten and Azouz, 2011).

In this paper, we also propose a simplified empirical model of the electrophysiological activity obtained from the infraorbital and vibrissal nerves. With this model implementation we aim not only to improve the interpretations of the results obtained from each methodological approach, but also to suggest alternative hypotheses and to make inferences about functional aspects of the system.

Materials and methods

Procedures

The procedure for accessing to the infraorbital and vibrissal nerves, the electrodes placement and the extracellular recording methods are described below.

Surgical procedure. Five Wistar adult male rats (300 g - 350 g) were used in this study. They were deeply anesthetized with urethane (1.5 g/Kg) and their temperature was maintained at 37° by a servo-controlled heating pad. Surgery consisted of exposing the infraorbital nerve. The zygomatic arch and the surrounding musculature from one side of the rat´s muzzle were removed in order to access the

nerve. We have used two recordings methods, the bipolar and the multielectrode ones, which are described below.

Bipolar method. The deep vibrissal nerve innervating one vibrissal follicle (Gamma vibrissa) was identified with a dissecting microscope. Then, it was proximally transected. To make sure that the transacted nerve did not affect the functionality of the vibrissal nerve during our recording time, we tested the decrease in the afferent nerve activity throughout time (data not shown). We concluded that the activity starts decreasing 1 hour after the nerve was sectioned, so we never exceeded this time in our experiments. Then, a bipolar electrode (insulated silver wire, 0.2 mm diameter) was used to register the multifiber afferent discharge of the selected vibrissal nerve (Fig. 1B). The electrodes as well as the nerves were immersed in a mineral oil bath during all the procedure. Nerve activity was registered and digitized at 20 kHz (sampling rate) by a Digidata 1322A (Axon Instruments). Movements of the Gamma whisker were monitored simultaneously by using a custom-made photoresistive sensor (Dürig et al, 2009).

Multielectrode method. A customized Utah Electrode Array, 6 x 6 microneedles (400 μm spacing), covering a surface of 2 mm x 2 mm millimetres, was placed on the infraorbital nerve (Fig. 1A). The Utah array was connected to an MPA32I amplifier (Multichannel Systems, MCS) and the extracellular recordings were digitized with an MCS analog-to-digital board. The data were sampled at a frequency of 20 KHz and digitally filtered out (100-3000 Hz).

All procedures described here were carried out in accordance with the recommendations of the Guide for the Care and Use of Laboratory Animals (National Research Council, NRC), the directive 2010/63/EU of the European Parliament and of the Council, the RD 53/2013 Spanish regulations on the protection of animals used for scientific purposes. In addition, they were approved by the Miguel Hernandez University Committee for Animal use in Laboratory.

Electrophysiological recordings

Afferent response was evoked by the application of controlled passive stimulations, which consisted of bending the whisker at different directions in the same plane (Fig. 1B).

Empirical modeling of electrophysiological activity

A nerve impulse, V_m, is propagated along a myelinated axon with a conduction velocity, υ, which is directly proportional to the diameter of the fiber (Ruch, 1973). This wave propagation is done in a saltatory mode, that is, the nerve impulse propagates from one node to another without amplitude attenuation making it possible for V_m to be observed in each of the Ranvier nodes but at different times (Fig. 2A) (Goldman and Albus, 1968). Then, a single fiber action potential (*SFAP*) can be observed through an extracellular electrode, *e*, placed near the fiber. *SFAP* is mathematically calculated by the following equation:

$$SFAP = \sum_{i=\infty}^{\infty} V_m\left(t - \frac{x_i}{\upsilon}\right).\Lambda_i \qquad (1)$$

$$\Lambda_i = \begin{cases} \Lambda_{\max}.\left(\dfrac{x_i - d_e}{d}\right) + \Lambda_{\max} & if \quad d_e - d \le x_i < d_e \\ -\Lambda_{\max}.\left(\dfrac{x_i - d_e}{d}\right) + \Lambda_{\max} & if \quad d_e \le x_i \le d_e + d \\ 0 & othercase \end{cases} \qquad (2)$$

Where Λ_i is a weighting factor that depends on the longitudinal and transverse conductivity of the interstitium, as well as the distance between the *i-th* node and the electrode (Andreasen and Struijk, 2002). In eq. 2, x_i is the distance from a predetermined origin at x = 0 to the *i-th* node, d_e is the distance from x = 0 to the extracellular electrode, *d* is the distance between the minimum and maximum attenuation of V_m (Fig. 2B). Λ_{max} is the minimum attenuation factor and it is given in the longitudinal position where the distance between the *i-th* node and the electrode is minimal (x_i position in Fig. 2B).

In the proposed model, we have considered *N* myelinated fibers, so Λ_{max} is a function of the perpendicular distance between the *j-th* fiber and the electrode. (df_j in Fig. 2C).

$$\Lambda_{\max}(df) = \begin{cases} 1 - \dfrac{df}{\Theta_b}\alpha & for \quad 0 \le df < \dfrac{\Theta_b}{\alpha} \\ 0 & othercase \end{cases} \qquad (3)$$

Where Θ_b is the diameter of the bundle of nerve fibers, and α is a constant related to the transverse conductivity of the interstitium. The eq. 3 is a straight line with negative slope and ordinate origin 1, i.e. $\Lambda_{max} = 1$ for $df = 0$ (represents the case of a fiber contacting the electrode). Likewise, $\Lambda_{max} = 0$, for $df = \Theta_b/\alpha$ (corresponding to the farthest fiber activity). Then, for N fibers, the CAP is computed as follows:

$$CAP_{e1} = \sum_{j=1}^{N} SFAP_j \qquad (4)$$

$$CAP = CAP_{e1} - CAP_{e2} \qquad (5)$$

Where $SFAP_j$ is the potential generated by the *j-th* fiber and CAP_{e1} is the compound action potential recorded by the electrode *e1* (Fig. 2C). Finally, the bipolar CAP is obtained with eq. 5.

Digital processing

Extracellular recordings were analyzed with several processing techniques according to the acquisition method.

Amplitude estimation (Root Mean Square – RMS). In previous studies, the amplitude of the afferent activity, with bipolar recordings, was related to the level of the mechanoreceptors' activation, so that higher RMS values would reveal a higher percentage of activation (Albarracín et al, 2006; Farfán et al, 2011). This is represented in this equation:

$$RMS = \sqrt{\frac{1}{N}\sum_{k=1}^{N}(x_k)^2} \qquad (6)$$

Where, x_k is *k-th* sample of the signal.

Time frequency analysis (spectrogram). A commonly used time-frequency representation is the short-time Fourier transform (Qian, 2002), defined as:

$$STFT_x(\tau, f) = \int_{-\infty}^{\infty} x(t) \times \omega(t-\tau) \times e^{-j \times 2\pi \times f \times t} df = \int_{-\infty}^{\infty} x(t) \times \omega_{t,f}^{*}(t) df \quad (7)$$

Where $\omega_{t,f}^{*}(t) = \omega(t-\tau) \times e^{-2\pi \times f \times t}$. *STFT* analyses the signal *x*(*t*) through a short-time window $\omega(t) = x(t) \times \omega(t-\tau)$, and then a Fourier transform is performed on this product using complex exponential basis functions. The square modulus of *STFT* is referred to as the spectrogram (Zhan et al., 2006).

$$SPEC_x(\tau, f) = |STFT_x(\tau, f)|^2 \quad (8)$$

Thus, the spectrogram of each multifiber activity recording is calculated by using these parameters: Hamming window length (HWL) of 200 samples, an overlap between segments of 97.5% (195 samples), and FFT length of 200. The frequency resolution of the spectrogram results in 100 Hz (sampling rate/HWL).

Event detection (CWT). When the whisker makes contact with a texture, or its movement changes because of passive stimulation, whisker motion signals report to the brain that the whiskers have been stimulated (Diamond et al. 2008). We have recently proposed that mechanical information about changes in the vibrissa position could be codified by electrophysiological events extracted from the corresponding vibrissal nerves (Farfán et al. 2013).

In this work, the events in the multifiber recordings were detected by using an event detection algorithm based on multiscale decomposition of the signal (Continuous Wavelet Transform—CWT). Nenadic and Burdick (2005) proposed the algorithm, and its detection methodology consists of a combination of several techniques stemming from multiresolution wavelet decomposition, statistics, detection theory and estimation theory. Next, we present the five major steps of the algorithm.

1. Multiscale decomposition of the signal using an appropriate wavelet basis.

A wavelet ψ is a function of finite energy and zero average which is normalized and centered in the neighborhood of the origin. From this function, also called mother wavelet, we can obtain a family of time-scale waveforms by translation and scaling

$$W_{a,b}(t) = \frac{1}{\sqrt{a}}\psi\left(\frac{t-b}{a}\right) \qquad a,b \in \mathbf{R} \qquad (9)$$

where $a > 0$ represents the scale and b the translation. The functions $\psi_{a,b}$ are called wavelets and they share the properties of the mother function (Nenadic and Burdick, 2005). The wavelet transform of an arbitrary function $x(t)$ is a projection of that function onto the wavelet basis.

$$T_x(a,t) = \int_R x(t)\psi_{a,b}(t)dt \qquad (10)$$

For event detection, it is important to choose a wavelet that is suitable for the signal of interest. The mother wavelet used in this paper belongs to the family of biorthogonal wavelets: 'bior1.5' (Daubechies, 1992) and it was chosen because its biphasic shape is reminiscent of compound action potentials.

The continuous wavelet transform defined by eq. 10, operates on a continuous set of scales and translations. Hence, the basis functions $\psi_{a,b}$ are not orthogonal and the representation of the signal x by its wavelet coefficients is redundant. Here we chose the set of basis function translations to be finite, where this set is determined by the sampling rate of the signal $f_s(kHz)$ and its duration $T(s)$, i.e., $b \in B$. $B=\{0,1,\ldots,k,\ldots,N\text{-}1\}$, and $N = Tf_s+1$ is the number of samples of the discrete signal (time series). Biophysical considerations were used to restrict the relevant scales of the wavelet basis functions. We used a limited set of scales $\boldsymbol{A}=\{a_0, a_1, \ldots, a_j, \ldots a_J\}$, where a_0 and a_J were determined from the signal sampling rate and the minimum and maximum event durations, denoted by W_{min} and W_{max}, respectively. We chose the intermediate scales $\{a_1, a_2, \ldots, a_{J-1}\}$ uniformly sampled between the two extremes a_0 and a_J with an arbitrary step. The wavelet decomposition scales were chosen in order to detect events with durations of 0.2 to 1.0 ms.

2. Separation of the signal and noise at each scale.

By applying the continuous wavelet transform, we obtained a multiscale representation of the signal in terms of its wavelet coefficients. If the discrete

observations *x* contain useful signals *s* and noise *w*, then the statistical properties of the wavelet coefficients will depend on those of the noise. In order to detect signals in an unsupervised way, we had to separate these coefficients by estimating the noise level σ in each coefficient from the sampled data. Then, the noise of each temporal series is eliminated by using simple threshold detection. The adaptive threshold, *T*, defined using the algorithm introduced in (Donoho, 1994) is given in equations (11) and (12).

$$T_j = \sigma_j \sqrt{2.\log_e(N)} \qquad (11)$$

Where *N* is the number of samples of the analyzed time series, σ^2_j is the variance of the noise coefficients *W(j,k)* at scale a_j, and T_j is the threshold of the time series. For a Gaussian random variable, it can be demonstrated that the median of its absolute deviation effectively estimates the standard deviation:

$$\hat{\sigma}_j = M\left\{\left|X(j,0) - \overline{X}_j\right|,...,\left|X(j,N-1) - \overline{X}_j\right|\right\}/0.6745 \qquad (12)$$

Where $\overline{X}_j$ is the simple mean of X_j and $M\{.\}$ denotes the sample median.

3. Events detection at a single scale.

The problem of detecting events in a noisy signal can be seen as a binary hypothesis testing problem, where under the null hypothesis, the signal is not present, and under the alternative, both signal and noise are present. Because of the transient nature of the signal, the alternative hypothesis, if true, will be so only for an interval of time, or equivalently for a subset of the discrete time. Moreover, multiple transients could be present, and these represent the main differences between the problems of classical signal detection and detection of action potentials. Nenadic and Burdick (2005) formulated the first step of the problem of detection as a sequential binary hypothesis test at each scale. The hypothesis-testing rule for each wavelet coefficient depends on the acceptable costs of false alarms and omissions and the prior probabilities of the two hypotheses (null and alternative). These factors are related to an acceptance threshold for the alternative hypothesis at each scale. In order to evaluate this threshold, the costs of false alarms and omissions should be specified. The algorithm proposed by Nenadic and Burdick (2005), uses a parameter *L* that is the result of a

reparameterization of the relationship between costs of false alarms and omissions (for more details see Nenadic and Burdick, 2005). For most practical purposes: $-0.2 \leq L \leq 0.2$. Larger L probably produces omissions, smaller L is more likely to produce false positives.

4. To combine the decisions at different scales.

Because they are highly localized in time, the samples corresponding to neural transients occupy contiguous subsets of the discrete time vector $\boldsymbol{B}$. This property of transients is often referred to as a temporal contiguity. Temporal contiguity translates into the contiguity of coefficients in the wavelet domain (Wang and Willett, 2001), i.e., the wavelet coefficients corresponding to the same transient tend to be neighbors in both time and scale. Since the algorithm used here uses the CWT with the basis functions of compact support roughly matched to the scale of neural transients, the temporal contiguity in the wavelet domain is inherently preserved. The scale contiguity follows from a broad frequency spread of a time-limited signal, so if a scale is thought of as an approximation of the frequency, a time-limited transient will be spread across many scales. The presence of noise, however, may obscure the picture at the scales that are not relevant. The scale contiguity can also be viewed in the present context as a cross-correlation (redundancy) of the wavelet coefficients (decisions) at different scales. The problem of redundancy and statistical decision criteria for event detection on multiple scales are formally described in Nenadic and Burdick (2005).

5. To estimate the arrival times of individual events.

In a noise-free environment, the wavelet basis function that provides the maximum correlation with the transient to be detected corresponds to a wavelet coefficient of maximum magnitude. The time associated with the translation index of the basis function with maximal coefficient can be taken as a good approximation to the occurrence time of the underlying transient. Because we chose the set of translations $\boldsymbol{B}$ with time resolution down to the sampling period, this approximation is essentially as good as the sampling period. Tracking of modulus maxima of the wavelet coefficients across scales was proposed for the detection of signal singularities (Mallat and Hwang, 1992). In a noisy environment, there is naturally a jitter associated with the location of this maximal coefficient. This jitter can be reduced by

averaging the locations of the maxima across different scales. This is basically the idea employed in procedures used to estimate the arrival times of individual events.

The MATLAB code of the method and a supporting tutorial are available at: http://robotics.caltech.edu/~zoran/Research/detection.html.

Spike Sorting via CWT. Afferent recordings obtained with microarray electrodes were subjected to offline spike sorting analysis. CAPs were extracted with Nenadic and Burdick algorithm and then were categorized according to their amplitudes.

Results

Electrophysiological recordings

The passive stimulation of a rat vibrissal shaft generates a massive follicle mecahnoreceptors discharge that travel through the primary afferents to its final destination in the somatosensory cortex.

Fig. 3A shows the gamma vibrissal nerve afferent activity evoked by a passive stimulation and recorded with a bipolar electrode. The vibrissal movement was simultaneously recorded by using a sensor displacement. The figure reveals morphological changes in the afferent signal related to the vibrissal displacement (inset right - Fig. 3A); as the vibrissa displacement magnitude increases, the amplitude of the discharge also increases. This amplitude increase could be related to the firing rate increase as a result of greater number of mechanoreceptors activated (Lichteinsten et al, 1990; Mitchinson et al, 2004; Lottem and Azouz, 2011).

A previous study established that an increase or decrease in the firing rate could evoke changes in the spectral content of the afferent signal (Pizá et al, 2014). Fig. 3B shows the time-frequency analysis of the afferent signal. The local maxima (100-1000 Hz) were detected between 120-200 ms in the spectrogram. This rising of the signal frequency components is associated with the maximum vibrissa deflection.

As was previously described, the mechanical information about changes in the vibrissa position could be codified by electrophysiological events extracted from the vibrissal nerves (Farfán et al. 2013). The events were detected by using an event detection algorithm based on multiscale decomposition of the signal. As Fig.3C

shows, events of 0.2, 0.6 and 1.0 ms in duration were detected. The detection algorithm yields a high rate of false detections when it is set to detect events shorter than 0.5 ms. Thus, events of 0.35 to 0.4 ms have a unipolar waveform, while events of 0.6 ms have a bipolar waveform (Fig. 3D).

The inter-events time showed an evident decline related to the rising of the vibrissal deflection. However, the lineal relation and the maximal sensitivity were obtained for events with 0.6 ms duration (Fig. 3E).

These results describe the stimulus-response relation in multifiber recordings protocol with passive stimulation; however, the activation of mechanoreceptors is not only evoked by the stimulus amplitude but also by the kinematic characteristics of the contact (Lottem and Azouz, 2011). To avoid the variation due to these characteristics, the stimuli were uniformly applied by using a step made by a transitory phase (around 20 ms) and a stationary phase. The amplitude deflection was around 5° (Fig. 4).

Fig 4 shows the afferent activity obtained with a microelectrode array (one channel) during a passive stimulation. The gamma vibrissa was deflected 5° to the up direction (middle area of Fig. 4). CAPs detected were grouped in two classes according to the amplitude differences. No significant differences were found in relation to the CAPs durations (around 0.5 ms). Transitory deflections (around 300 ms) did not evoke CAPs, suggesting the presence of slowly adapting fibers.

Empirical modeling of afferent recordings

Electrophysiological events with different durations, amplitude and temporal occurrence were detected with a bipolar multifiber recording protocol (Fig. 3) (Farfán et al, 2013).

The model described here, was adjusted to the temporal features of events detected in both bipolar and monopolar recordings, in order to reveal its origin and to improve the interpretation of the results obtained. It is important to make a consideration about the stimulation. The model is based on electrically-evoked responses and the discharges in our experiments were generated with mechanical

stimulation. It does not represent a substantial difference since the CAP morphology depends on propagation characteristics and not on how it is generated. Instead, it is crucial to rely on anatomical data (i.e. bundle diameter, amount of myelinated fibers, etc.) and the electrodes position.

Fig. 5A shows simulations that were performed under the following considerations: the recording electrodes were placed at different distances from the stimulation electrode (10000-20000 μm), the number of fibers was 4000, the bundle diameter was 1500 μm and the inter-nodal distance was 2000 μm. For simplicity, it was considered that the mechanical stimulation evoked nerve impulses (unitary amplitude and 0.5 ms duration) in each of the fibers. The monopolar CAPs recorded by e_1 and e_2 electrodes are shown in Fig. 5B-E (red and blue lines, respectively). The position of electrode e_1 was settled in d_{e1}=10000μm, while electrode e_2 in d_{e2}= 12500, 15000, 17500 and 15000 μm. The simulation protocol shows that the duration and amplitude of bipolar CAPs (shaded areas) increases as distance between e_1 and e_2 increase (Fig. 5B-E).

We have made another set of simulations that are shown in the Fig. 6. If the weighting factor (Λ_i) is varied, the duration and amplitude of the CAPs is affected by the longitudinal conductivity (amount of nodes included) (Fig. 6A). On the other hand, if the e_1 and e_2 positions (with $|d_{e1} - d_{e2}|$=2000 μm) are the simultaneously changed, it cause more significant morphological changes in the CAPs (Fig. 6B).

The amount of electrically active mechanoreceptors is another factor that affects the CAPs amplitude. Fig. 6C shows simulations obtained varying Λ_{max} that is related to the transverse conductivity of the interstitium and the perpendicular distance between the fibers and the electrode. Increases in this parameter produce decreases in the relative amplitude of differential CAPs. The durations of CAPs is not affected.

Figs. 7A and 7B show the simulation schemes that fitt the model to the waveforms of CAPs obtained with the two recording methods. The bipolar CAPs were adequately adjusted using the following parameters: d_{e1}=15000μm, d_{e2}=23000μm ($|d_{e1} - d_{e2}|$=8000 μm), Λ_j = 5 nodes, Λ_{max}(df=0) =1, number of fibers = 200, bundle diameter 1250μm. The amount of fibers, bundle diameter and d_{e1} parameters were kept constant for CAP recorded with the microarray electrode.

However, Λ_j and Λ_{max} changed according to the consideration that the main difference between the two protocols is the size of the recording electrodes, which results in large differences in the interface impedance. The higher the interface impedance, the lower the electrode action field, and therefore only the activity of the nearby fibers was recorded. This was simulated through Λ_j.

The bipolar CAPs were detected and grouped according to their durations and amplitudes. Thus, for example, it was possible to register three morphologically different CAPs (Fig. 7C) in an experimental protocol. The model was empirically adjusted using constant parameters, such as number of fibers = 200, bundle diameter 1250μm, and other parameters such as inter-electrode distance ($|d_{e1} - d_{e2}|$), Λ_j and Λ_{max}(df=0). The inter-electrode distance and Λ_j parameters were tuned to fit the experimental CAPs durations, while Λ_{max}(df=0) was tuned to fit the amplitude.

Directional response

Another set of experiments about of directional response were made in order to evaluate the processing techniques and the modeling proposed.

Fig. 8 shows afferent discharges evoked by vibrissa deflections at different directions and recorded with the bipolar method. As we have already mentioned, the transitory and stationary phase present different patterns of discharge. Thus, the amplitude and the frequency features were analyzed separately. The RMS values show directional sensitivity in the deflection transitory phase which is characterized by a higher activation for 90°, 135° and 180° directions (Fig. 8A). The stationary phase shows higher activation only for 135°; for other directions it stays without significant changes. This figure also shows the spectrograms obtained. The maximum-energy frequency component (Fmean) is located in the bandwidth 100 – 1000 Hz for both stimulus phases. The polar diagrams show that, in the case of the transitory phase, the Fmean is 600 Hz for 0°, 90°, 135° and 180°, but for 270° it is around 200 Hz. In the case of the stationary phase, the Fmean decreases for 135° and 180° (550 and 400 Hz) but increases to 550 Hz for 270°.

Events detected from the afferent discharge and their firing rates are represented in the Fig. 8B. The events of 0.6 ms have the highest firing rate at 90° for

the transitory and stationary phases, 300 events/sec and 150 events/sec, respectively. Events of 1.0 ms showed a similar behavior but with a greater directional acuity.

Our results about the directional response in the vibrissal system could partially differ from those described by other authors (Lichtenstein et al, 1990). This is because the recordings analyzed here are the average activity of many axons.

The empirical model implementation allowed us to estimate the relative percentage of active fibers in each stimulation direction and to make inferences about the proportion of slow and fast adapting responses involved.

We also analyzed the directional sensitivity for recording obtained by using multiarray electrodes. The algorithm detected the CAPs and they were grouped according to their amplitude in R1 and R2 responses (Fig 9A). Then, the firing rate was calculated and represented in the figure according to the different directions applied. The global firing rate was higher for 180º (150 CAPs/sec), followed by 135° (130 CAPs/sec) and 270° (120 CAPs/sec). For other directions, the mean firing rate was 70 CAPs/sec (Fig 9A). The R2 group also showed a higher firing rate for the 270º (43 CAPs/sec). On the other hand, events with lower amplitude (R1 group) showed the highest firing rate for 135º and 180º (around 100 CAPs/sec). In brief, CAPs detected by amplitude showed different directional characteristics that explain the global pattern observed in the afferent activity during the passive stimulation. Results obtained from other animal showed higher firing rate for deflections to180° (Fig. 9B).

Discussion

In neurophysiology the interpretation of the results depends on multiple factors but especially on the methodological features. In this sense, extracellular recordings often represent a challenging not only in extracting correctly the information but also in the correct interpretation. Because of this, the use of specific data processing methods is highly advisable.

In this paper, we address the analysis of two electrophysiological methodologies: the bipolar and multielectrode recordings.

The bipolar recording method does not require complex equipment for its implementation because the recording electrodes are relatively large (small contact

impedance). It does require, however, complex processing techniques for a better interpretation of the data. The techniques based on microelectrodes, on the other hand, need equipment with more complex technological requirements, such as series resistance compensation, capacitance compensation, among others. This research highlights the advantages and disadvantages of using electrophysiological techniques based on bipolar methods and those based on microelectrodes array. Both methods were implemented to study the sensorial information carried by the vibrissal afferents nerves when the vibrissae are passively stimulated (Lichtenstein et al, 1990; Mosconi et al, 2010).

A variety of responses (slowly adapting, rapidly adapting and slowly adapting low threshold) are evoked in the follicle-sinus-complex when the vibrissae are passively stimulated (Mitchinson et al, 2004; Kwegyir-Afful et al, 2008; Lotten and Azouz, 2011). Thus, studying these responses in the vibrissal nerves represents a great methodological challenge. Lichtenstein et al, (1990) demonstrated that the responses evoked in the follicle-sinus-complex depend on the direction of the mechanical stimulation (directional response of the vibrissal system). Here, we show that it is possible to study the directional response through electrophysiological techniques in the vibrissal nerves, and that the set of features extracted from the recordings (energy, frequency, discrete events, CAPs) could provide anatomical and functional descriptions of the system.

The CAPs modeling was possible through the adjustment of anatomical parameters of the vibrissal nerve, spatial arrangement of the recording electrodes, and indirectly of its geometric dimensions. The proposed model allows not only the association between anatomical and functional characteristics at the afferent level (Wijesinghe et al, 1991), but also the prediction of changes in the CAPs morphology when the arrangement and the geometry of the electrodes change. It also makes it possible to predetermine the distances between the recording electrodes and the position where V_m potentials originate, in order to observe the contribution of fast and slow nerve fiber groups (McComas, 2011, Pizá et al, 2016). The experimental validation of the model was performed by using an electrical stimulation protocol and recording the evoked CAP obtained from a frog's sciatic nerve and from a rat's vibrissal nerve (Pizá et al, 2016).

The CAPs modeling requires a priori shape knowledge of the nerve impulse, V_m, which propagates along each fiber of the beam. This particularity allows more complex morphologies of V_m to be considered, thus giving the model greater flexibility. Another characteristic is that the model supposes a point of contact, between the electrode and the tissue, with interface impedance equal to zero, which simplifies its formulation considerably. However, an improvement could be possible by using non-linear approaches to model the contact area, for example, through the electrode-electrolyte interface theory (Ruiz and Felice, 2007).

The comparative study proposed in this work reveals a close relationship between the electrophysiological techniques and the processing methods necessary to extract sensory information. This relationship, which is not often documented, is the result of maximizing the extraction of information from recordings of sensory activity. The compendium of processing techniques used here, is not, and does not pretend to be, the only one for the study of afferent sensory activity, but it is rather the result of previous research in the area (Albarracín et al, 2006; Farfán et al, 2011; Farfán et al, 2013; Pizá et al, 2014; Alegre-Cortés et al, 2016).

Conclusions

This work presents the comparative study of two electrophysiological methods. Both of them were used in an experimental protocol aimed at studying the tactile information of the rat's vibrissal system when their whiskers are mechanically stimulated. The morphology of the evoked CAPs was analyzed by using an empirical model, which allowed establishing anatomical/functional relationships and highlight the most relevant features of nerve conduction in myelinated fibers. In addition, the analysis techniques used to functionally characterize the rat's vibrissal system revealed a close qualitative relationship between the electrophysiological methods and the complexity of the analysis techniques. Finally, this study gathers a compendium of known procedures that were implemented for the first time in the analysis of the electrophysiological activity recorded in the vibrissal nerves.

Conflict of Interest

None declared.

Acknowledgments

This work is supported in part by Consejo Nacional de Investigaciones Científicas y Técnicas (CONICET), Consejo de Investigaciones de la Universidad Nacional de Tucumán (CIUNT) and Institutional funds from Instituto Superior de Investigaciones Biológicas (INSIBIO). Also, by a grant MAT2015-69967-C03-1-R from the Spanish Government, by the Bidons Egara Research Chair of the University Miguel Hernández, and by a research grant of the Spanish Blind Organization (ONCE).

We also want to thank Prof. Gilda Moreno for her helps in the manuscript language edition.

References

Ahissar E, Sosnik R and Haidarliu S (2000) Transformation from temporal to rate coding in a somatosensory thalamocortical pathway. Nature, 406(6793): 302-306.

Albarracín AL, Farfán FD, Felice CJ, Décima EE (2006) Texture discrimination and multi-unit recording in the rat vibrissal nerve. BMC Neuroscience, 7:42.

Alegre-Cortés J, Soto-Sánchez C, Pizá AG, Albarracín AL, Farfán FD, Felice CJ and Fernández E (2016) Time-Frequency analysis of neuronal populations with instantaneous resolution based on Noise-Assisted Multivariate Empirical Mode Decomposition. Journal of Neuroscience Methods 267: 35-44.

Andreasen LNS and Struijk JJ (2002) Signal strength versus cuff length in nerve cuff electrode recordings. IEEE Transactions on Biomedical Engineering 49(9):1045–1050.

Branner A and Normann RA (2000) A multielectrode array for intrafascicular recording and stimulation in sciatic nerve of cats. Brain Res. Bull. 51 293–306.

Brecht M, Preilowski B, Merzenich MM (1997) Functional architecture of the mystacial vibrissae. Behavioural Brain Research, 84(1–2): 81-97.

Castro-Alamancos MA (2002) Different temporal processing of sensory inputs in the rat thalamus during quiescent and information processing states *in vivo*. J. Physiol. 539: 567–578.

Daubechies I (1992) Ten Lectures on Wavelets. Philadelphia, PA: SIAM.

Diamond M E, von Heimendahl M and Arabzadeh E (2008) Whisker-mediated texture discrimination. Plos Biology 6(8), e220.

Donoho DL (1994) Nonlinear wavelet methods for recovery of signals, densities, and spectra from indirect and noisy data. Proc. Sympos. Appl. Math. 173–205.

Dürig F, Albarracín AL, Farfán FD, Felice CJ (2009) Design and construction of a photoresistive sensor for monitoring the rat vibrissal displacement. Journal of Neuroscience Methods, 80(1): 71-76.

Farfán FD, Albarracín AL, Felice CJ (2011) Electrophysiological characterization of texture information slip-resistance dependent in the rat vibrissal nerve. BMC Neuroscience, 12:32.

Farfán FD, Albarracín AL, Felice CJ (2013) Neural encoding schemes of tactile information in afferent activity of the vibrissal system. Journal Computational Neuroscience, 34: 89–101.

Gibson JM and Welker WI (1983) Quantitative studies of stimulus coding in first-order vibrissa afferents of rats. 1. Receptive field properties and threshold distributions. Somatosens. Res., 1: 51–67.

Gibson JM (1987) A quantitative comparison of stimulus-response relationships of vibrissa-activated neurons in subnuclei oralis and interpolaris of the rat's trigeminal sensory complex: receptive field properties and threshold distributions. Somatosens. Res. 5(2): 135-55.

Goldman L and Albus JS (1968) Computation of Impulse Conduction in Myelinated Fibers; Theoretical Basis of the Velocity-Diameter Relation. Biophysical Journal 8(5): 596–607.

Kleinfeld D, Ahissar E and Diamond ME (2006) Active sensation: insights from the rodent vibrissa sensorimotor system. Current Opinion in Neurobiology, 16: 435–444.

Krupa DJ, Matell MS, Brisben AJ, Oliveira LM and Nicolelis MAL (2001) Behavioral Properties of the Trigeminal Somatosensory System in Rats Performing Whisker-Dependent Tactile Discriminations. The Journal of Neuroscience, 21(15): 5752–5763.

Kyriazi HT, Carvell GE and Simons DJ (1994) OFF response transformations in the whisker/barrel system. J. Neurophysiol., 72(1): 392-401.

Kwegyir-Afful E, Marella S and Simons DJ (2008) Response properties of mouse trigeminal ganglion neurons. Somatosensory & Motor Research 25(4): 209-21

Lichtenstein SH, Carvell GE and Simons DJ (1990) Responses of rat trigeminal ganglion neurons to movements of vibrissae in different directions. Somatosensory Motor Research 7(1): 47-65.

Lottem E and Azouz R (2011) A unifying framework underlying mechanotransduction in the somatosensory system. Journal Neurosccience 31(23): 8520-32.

Mallat S and Hwang WL (1992) Singularity detection and processing with wavelets. IEEE Trans. Inform. Theory, 38 (2): 617-643.

McComas AJ (2011) Galvani's Spark: The Story of the Nerve Impulse. New York, USA: Oxford University Press.

Merighi A and Carmignoto G eds. (2002) Cellular and Molecular Methods in Neuroscience Research. Springer Science+Business Media New York.

Mitchinson B, Gurney KN, Redgrave P, Melhuish C, Pipe AG, Pearson M, Gilhespy I and Prescott TJ (2004) Empirically inspired simulated electro-mechanical model of the rat mystacial follicle-sinus-complex. Proceedings of the Royal Society B: Biological Sciences, 271: 2509-2516.

Mohanty SK and Lakshminarayananan V (2015) Optical Techniques in Optogenetics. Journal of modern optics, 62(12): 949-970.

Mosconi T, Woolsey TA and Jacquin MF (2010) Passive vs. active touch-induced activity in the developing whisker pathway. Eur J Neurosci. 32(8): 1354–1363.

Nenadic Z and Burdick JW (2005) Spike detection the continuous wavelet transform. IEEE Transactions on Biomedical Engineering 52(1): 74–87.

Nicolelis MAL, Chapin JK and Lin RC (1995) Development of direct GABAergic projections from the zona incerta to the somatosensory cortex of the rat. Neuroscience, 65: 609-631.

Pizá AG, Farfán FD, Albarracín AL, Lucianna FA, Soletta JH and Felice (2016) A Simplified Empirical Modeling of Electrophysiological Activity in a Bundle of Myelinated Nerve Fibers. IEEE Latin America Trans. 14, 3345-3350.

Pizá AG, Farfán FD, Albarracín AL, Ruiz GA and Felice CJ (2014) Discriminability measures and time-frequency features: an application to vibrissal tactile discrimination. Journal of Neuroscience Methods 233: 78-88.

Qian S (2002) Introduction to time–frequency and wavelet transforms. Prentice Hall PTR: New Jersey.

Rangavajla G, Mokarram N, Masoodzadehgan N, Pai SB, Bellamkonda RV (2014) Non-Invasive Imaging of Peripheral Nerves. Cells, tissues, organs. 200(1): 69-77.

Ruch TC (1973) Physiology and biophysics, 20th ed. Philadelphia: W.B. Saunders Company.

Ruiz GA and Felice CJ (2007) Non-linear response of an electrode–electrolyte interface impedance with the frequency. Chaos, Solitons & Fractals 31(2): 327–335.

Shoykhet M, Doherty D and Simons D (2000) Coding of deflection velocity and amplitude by whisker primary afferent neurons: implications for higher level processing. Somatosens. Motor Res. 17, 171–180.

Simons DJ and Carvell GE (1989) Thalamocortical response transformation in the rat vibrissa/barrel system. J. Neurophysiol., 61(2): 311-30.

Vertes RP and Stackman RW eds. (2011) Electrophysiological recording techniques. Springer Science+Business Media, LLC, Humana Press.

Vogt N (2018) Transformative electrophysiology. Nature Methods, 15, 31.

Wang Z and Willet PK (2001) All-purpose plug-in power-law detectors for transients signals. IEEE Trans. Signal Processing. 49 (11): 2454-2466.

Wark HAC, Sharma R, Mathews KS, Fernandez E, Yoo J, Christensen B, Tresco P, Rieth L, Solzbacher F, Normann RA and Tathireddy P (2013) A new high-density (25 electrodes/mm^2) penetrating microelectrode array for recording and stimulating sub-millimeter neuroanatomical structures. J. Neural Eng. 10(4): 045003.

Watkins PT, Santhanam G, Shenoy KV, Harrison RR (2004) Validation of adaptive threshold spike detector for neural recording. Engineering in Medicine and Biology Society. EMBS‘ 04, in 26th Annual International Conference of the IEEE, Vol. 2, San Francisco, CA, 4079–4082.

Wijesinghe RS, Gielen FL and Wikswo JP (1991) A model for compound action potentials and currents in a nerve bundle. I: The forward calculation. Ann Biomed Eng, 19(1): 43–72.

Zhan Y, Halliday D, Jiang P, Liu X, Feng J (2006) Detecting time-dependent coherence between non-stationary electrophysiological signals – A combined statistical and time–frequency approach. Journal Neuroscience Methods, 156(1–2): 322–32.

Zucker E and Welker WI (1969) Coding of somatic sensory input by vibrissae neurons in the rat's trigeminal ganglion. Brain Res., 12: 138-156.

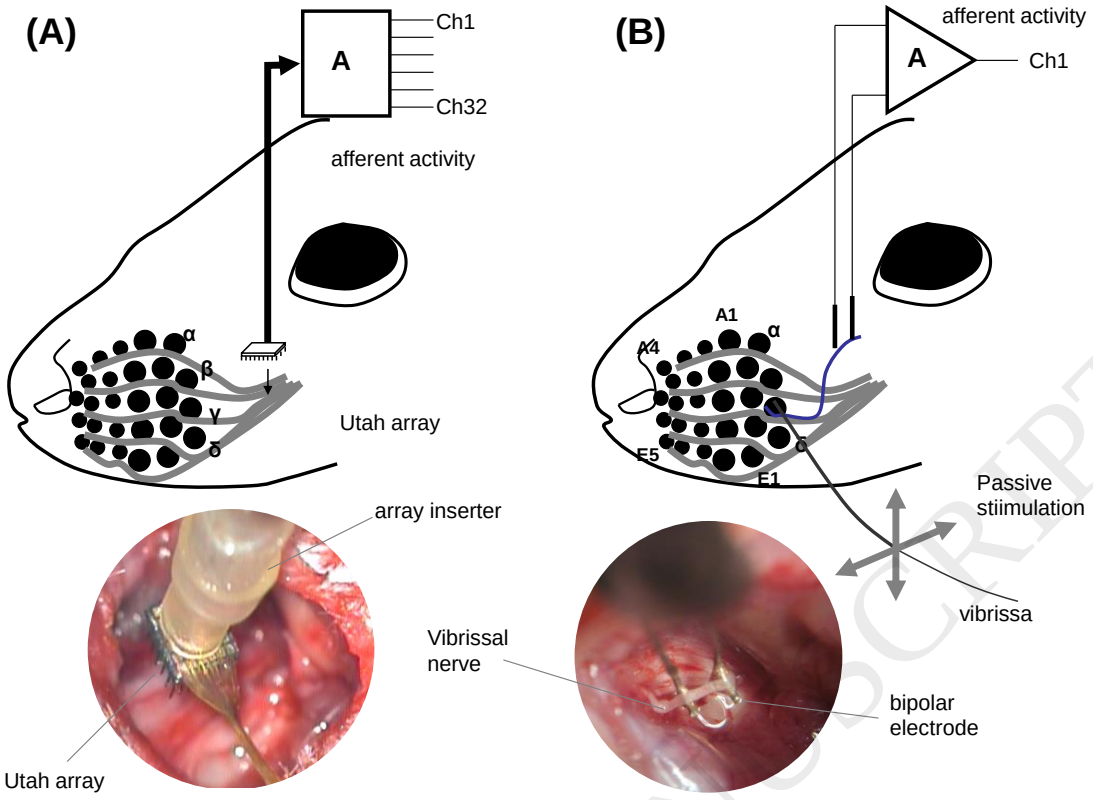

Fig. 1 Schematic representation and photographs of the recording methods used. (A) Multielectrode method and (B) Bipolar method. Vibrissa passive stimulation was applied in the same way in both cases.

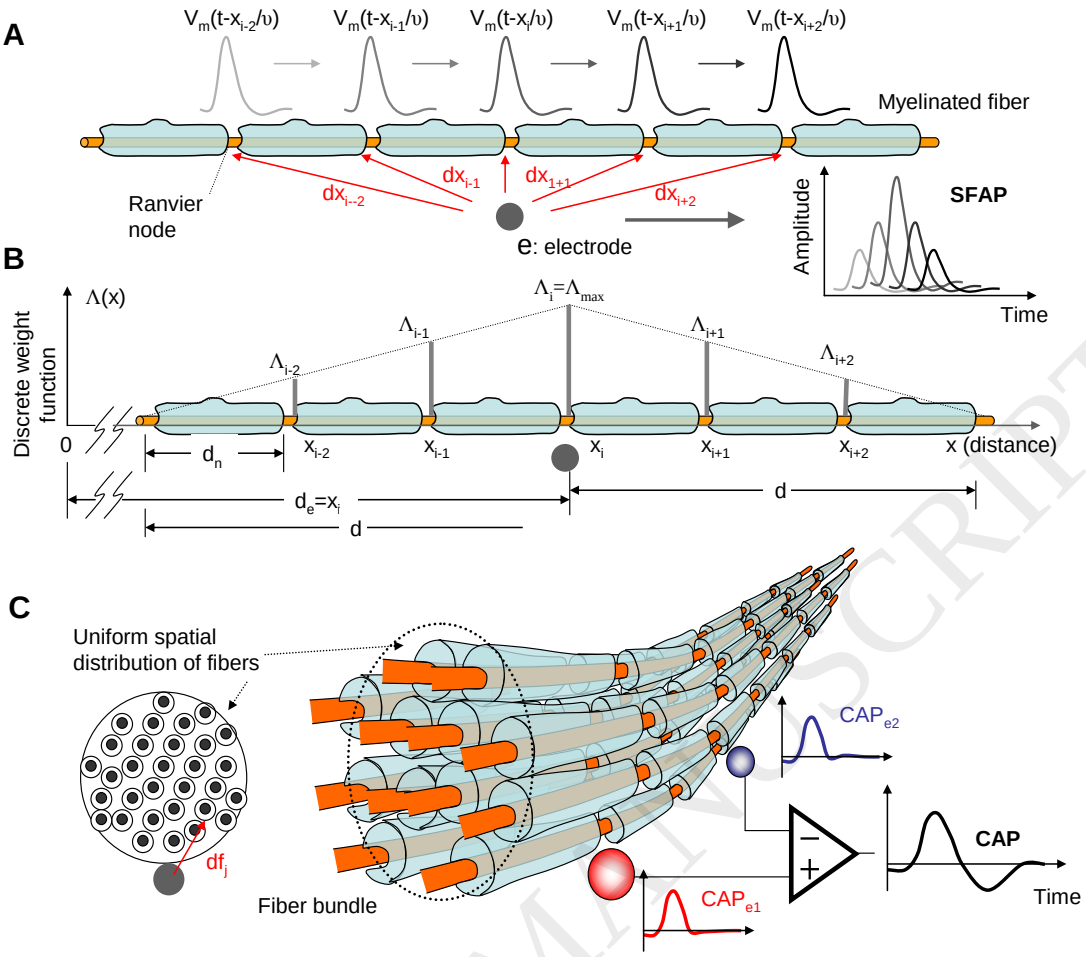

Fig. 2. Empirical model of the discharge in a bundle of myelinated fibers. (A) SFAP model recorded by the electrode, *e*. The action potential attenuation V_m, depends on the distance between the *i-th* node and the recording electrode. (B) Attenuation factor, which depends on the distance to the recording electrode. The origin, x=0, is where the action potential V_m is generated. (C) Diagram that illustrates the model. The spatial arrangement of the fibers is considered as a uniform distribution throughout the cross section of the bundle.

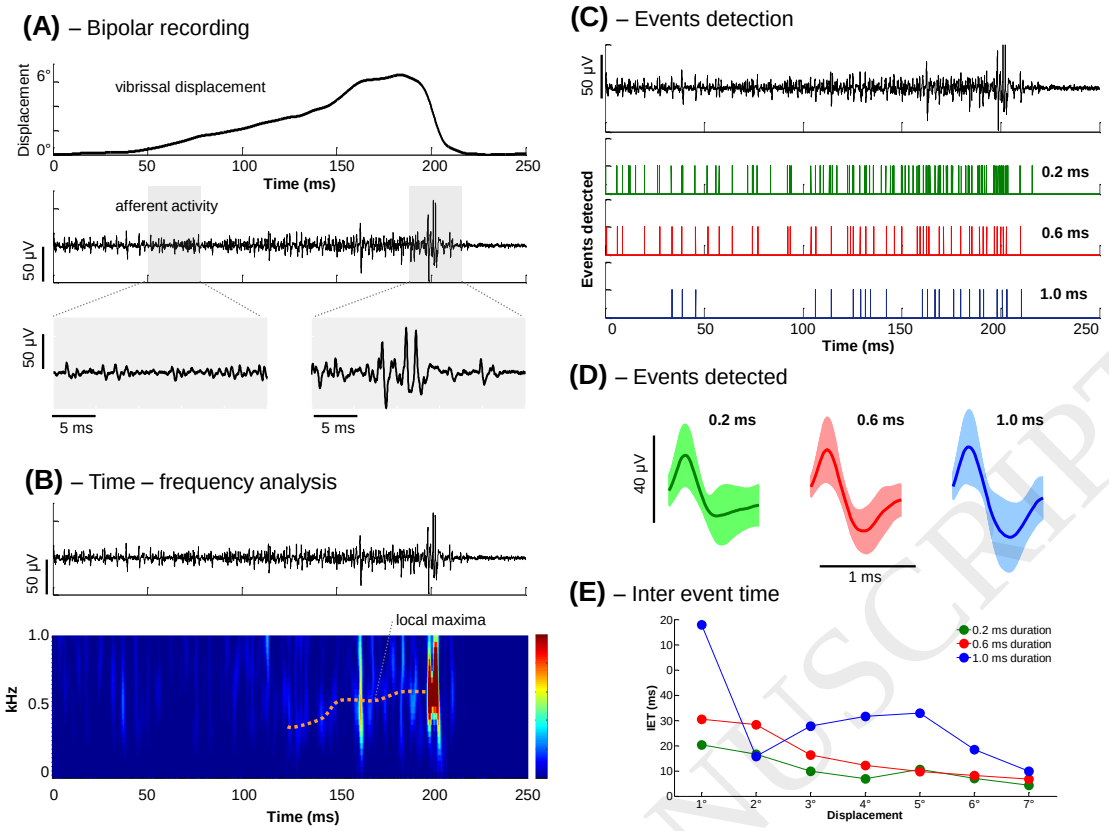

Fig. 3. Bipolar recordings and processing. (A) Bipolar recordings obtained from gamma vibrissal nerve and the vibrissa displacement applied (passive stimulation). (B) Time-frequency analysis. The spectrogram was obtained by using the following setting: window of 200 samples, 195 samples overlapped and NFFT = 1000 points. The local maxima components (100–1000 Hz) were obtained (orange line points). (C) Bipolar recording and detected events of different durations. (D) Events detected. (E) Inter-event time (IET) analysis. IET averages obtained from five similar vibrissal displacements.

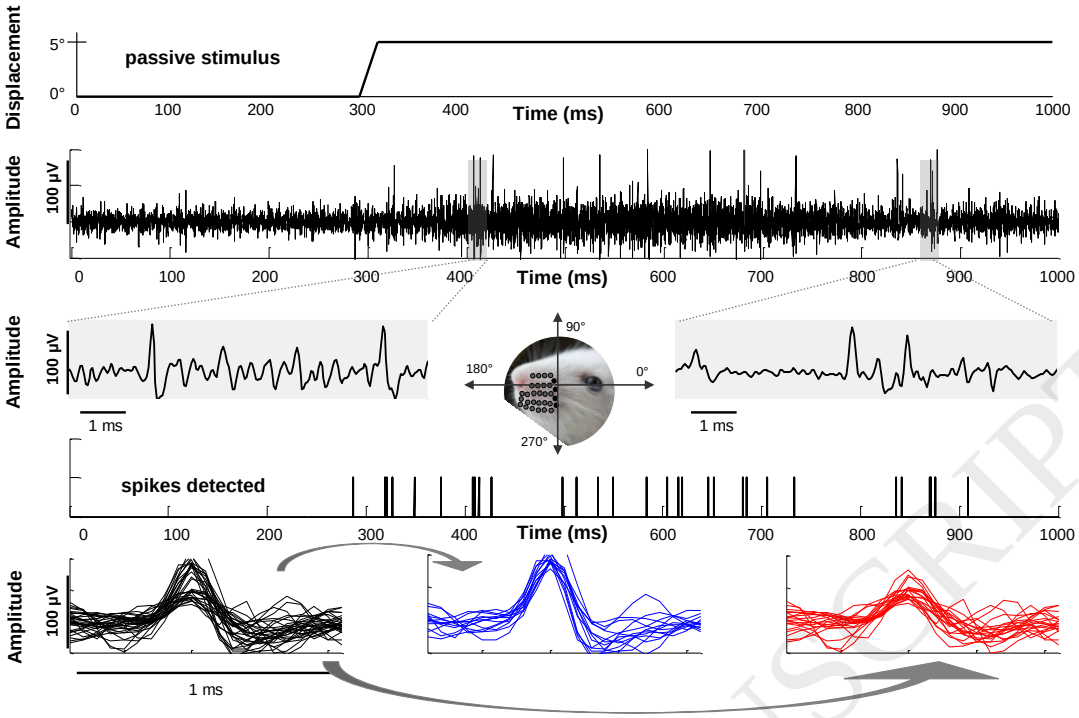

Fig. 4. Afferent recording obtained with microarray electrode (one channel). The gamma vibrissa was deflected 5°. The vibrissa displacement and evoked response are shown at the top. Details of the CAPs are shown in the shaded areas. Temporary locations of detected CAPs are shown below. The clustering of CAPs sorting procedure is at the bottom.

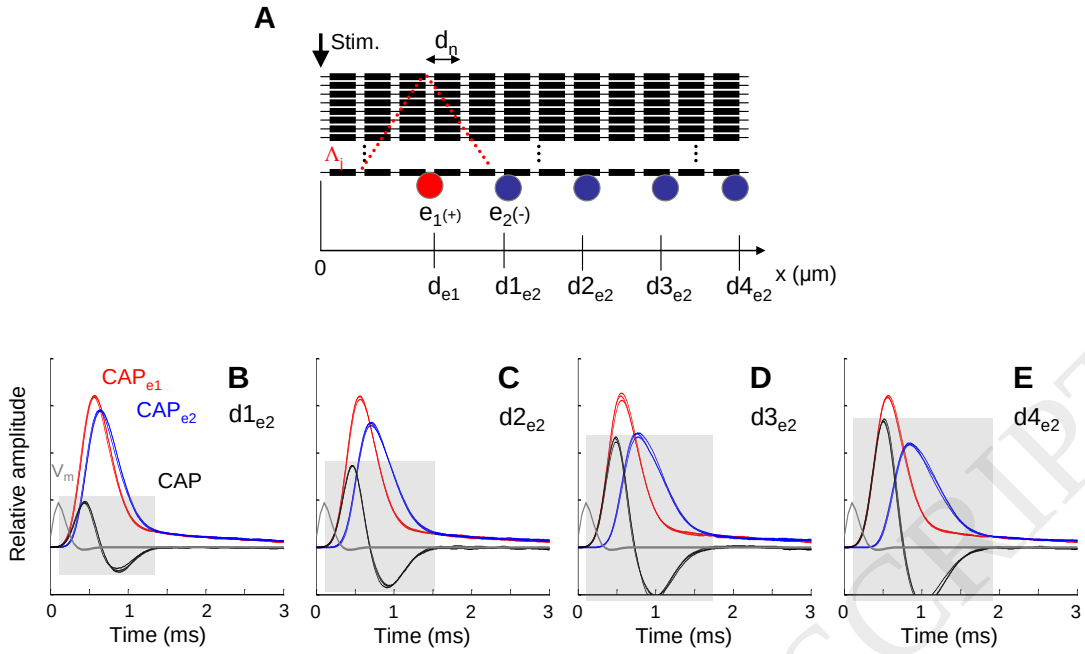

Fig. 5. Empirical model: simulations of a nerve multifiber discharge. (A) Scheme of electrodes arrangement respect to the bundle. The nerve impulses are generated in x=0 (e.g. due to a supramaximal stimulation) and they propagate along fibers with specific conduction velocities. The simulations were performed considering the following specifications: d_{e1}=10000 μm, $d1_{e2}$=12500 μm, $d2_{e2}$=15000 μm, $d3_{e2}$=17500 μm and $d4_{e2}$=20000 μm. (B) Monopolar (red and blue) and bipolar CAPs (black). The nerve impulse that travels along the fibers is in gray line. The CAP amplitudes are relative values to the V_m amplitude. Anatomical features considered for the simulated nerve: bundle diameter 1500 μm, 10 nodes, d_n=2000 μm. Electrodes positions of e_1 and e_2 : 10000 μm and 12500 μm, respectively. Five simulations were done. (C-F) Idem to A but changing the e_2 electrode position. (C) $d1_{e2}$=12500 μm. (D) $d2_{e2}$=15000 μm. (E) $d3_{e2}$=17500 μm and (F) $d4_{e2}$=15000 μm.

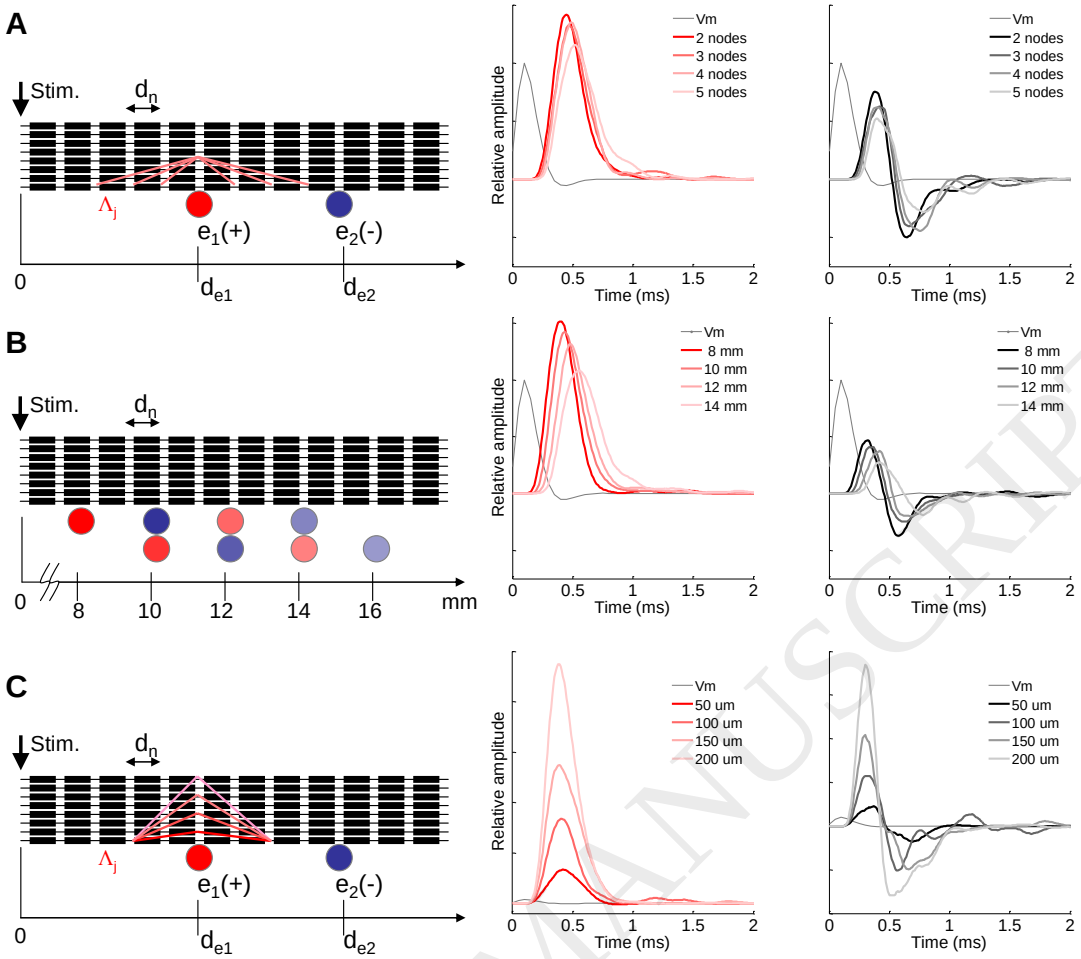

Fig. 6. Morphological changes of the CAPs by varying the model parameters. (A) Monopolar CAPs (red scale) and bipolar CAPs (gray scale) for different Λ_j values. Λ_j reaches longitudinal openings of 4, 6, 8 and 10 nodes. (B) Monopolar and bipolar CAPs obtained from electrodes placed at different positions. The inter-electrode distance was 2000 µm in this case. (C) Monopolar and bipolar CAPs for different α values. This parameter is related to the transverse conductivity of the interstitium and it is defined in eq. 3. The effect of the interstitial conductivity was qualitatively evaluated by varying Λ_{max} so that Λ_{max}(df=0) was equal to 1, 3/4, 1/2 and 1/4. These values correspond to transversal coverage of 200, 150, 100 and 50 µm, respectively.

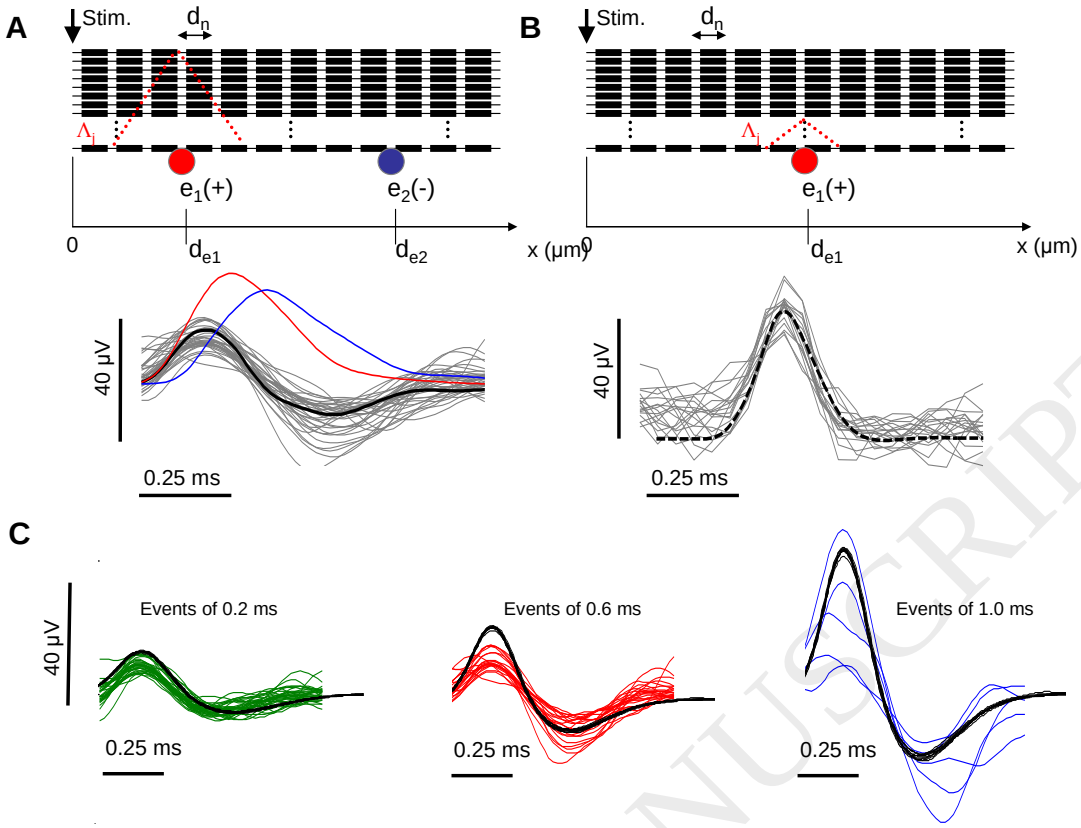

Fig. 7. Fitting the model to the experimental data. (A) Scheme of the simulation and the fitting made for potentials detected in the bipolar recordings. The experimental data are in gray lines, while the model results in black lines. (B) Idem to A, but using potentials detected in the monopolar recordings. (C) Fitting for three different potentials detected in a bipolar recording of afferent activity.

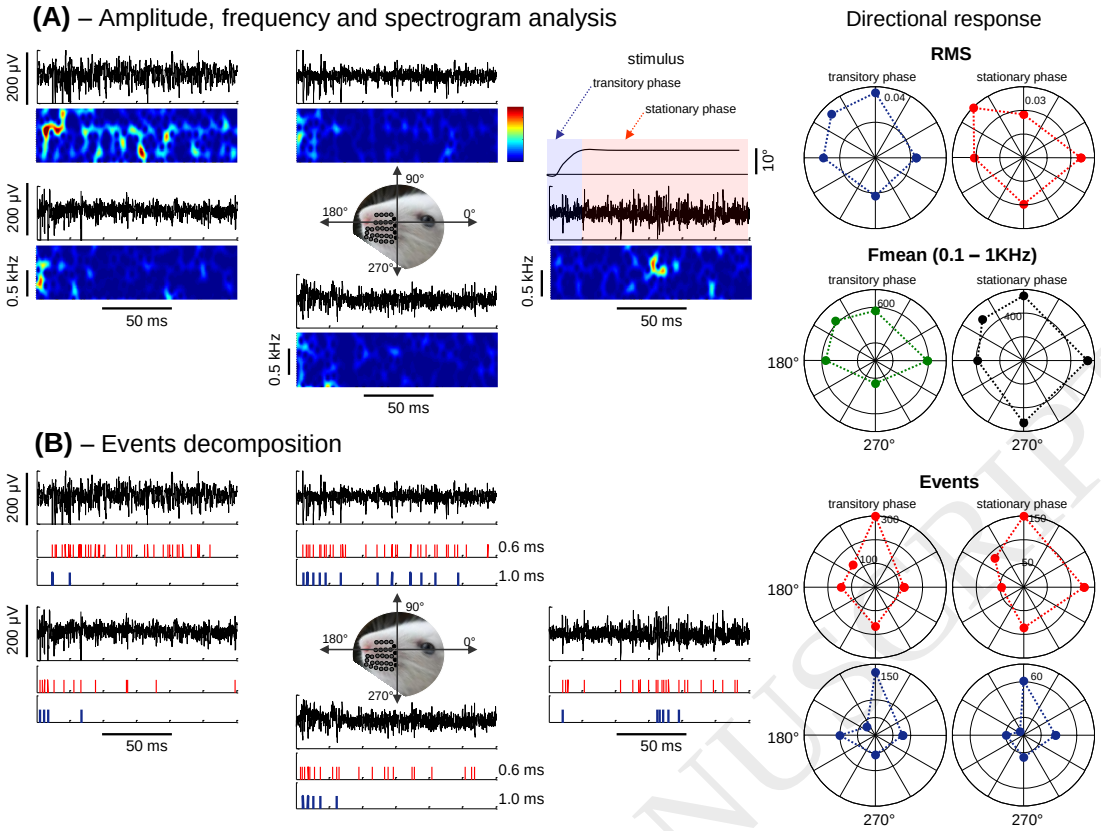

Fig. 8. Directional responses recorded with bipolar method. (A) Afferents recordings evoked by passive stimulus at different directions. The passive stimulus has a transitory phase (0 – 30 ms approx.) and a stationary phase (30 – 150 ms approx). The spectrograms of each recording are also shown here. The RMS values were calculated and represented in polar coordinates (directional responses). The average maximum-energy frequency component (Fmean) into 0.1 – 1 kHz bandwidth was obtained from the spectrogram, and its value is also represented in polar coordinates (on the right). (B) Afferent signal and events detected by using the CWT algorithm. The cumulative event count (CEC) was obtained for both transitory and stationary phases and represented in polar coordinates (on the right).

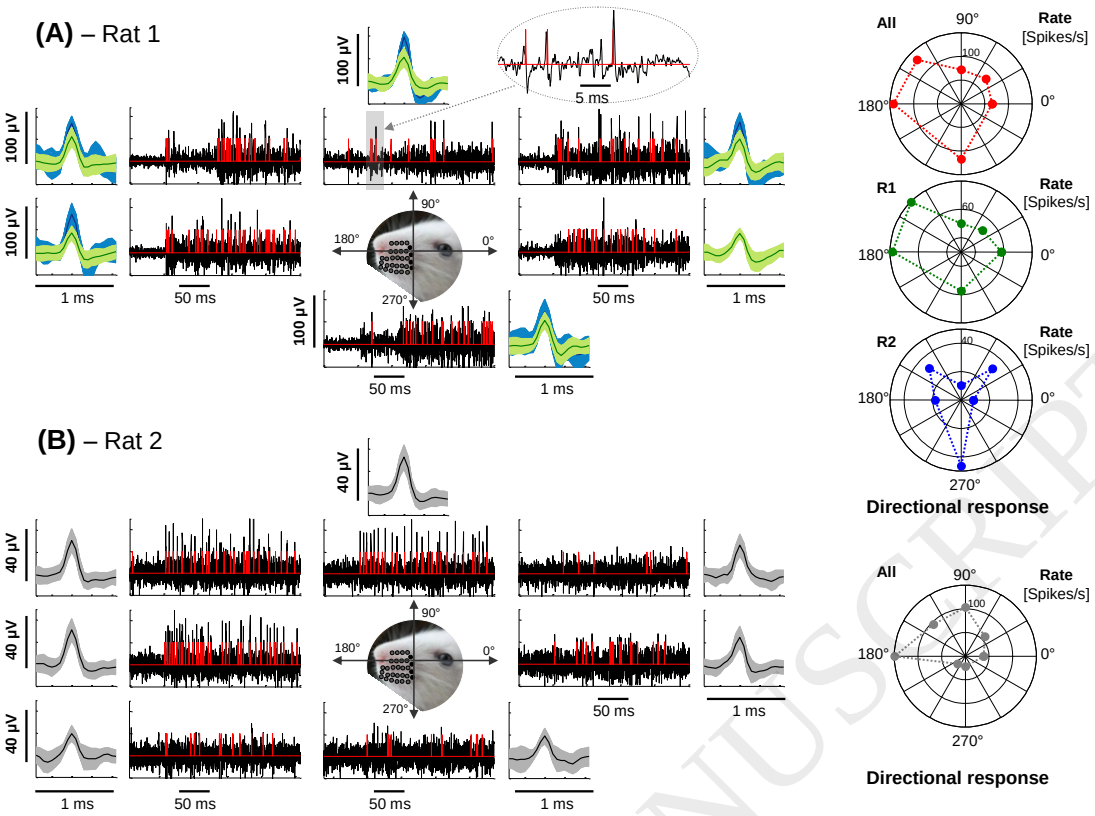

Fig. 9. Directional responses recorded with microarray method. (A) Extracellular recordings obtained during passive stimulation applied to E1 vibrissa at different directions. The binary signal (in green and blue) represents the detected CAPs from raw signal. Two groups of responses were sorted according to energy features: R1 responses (green) and R2 responses (blue). All responses detected (red), R1 responses and R2 responses are represented in polar diagrams (right). (B) Idem to A. No morphological differences were found. Directional responses are represented on the right.